J. Schreiber, E.M. Nanos, F. Campagnolo, C.L. Bottasso
Verification and Calibration of a Reduced Order Wind Farm Model by Wind Tunnel Experiments
Journal of Physics: Conference Series, Vol. 854, N. 1, 2017, 012041 (11 pages)
doi:10.1088/1742-6596/854/1/012041

The final publication is available at http://dx.doi.org/10.1088/1742-6596/854/1/012041

IOP Conf. Series: Journal of Physics: Conf. Series **854** (2017) 012041 doi:10.1088/1742-6596/854/1/012041

Verification and Calibration of a Reduced Order Wind Farm Model by Wind Tunnel Experiments

J Schreiber[1], E M Nanos[1], F Campagnolo[1], C L Bottasso[1,2]

[1] Wind Energy Institute, Technische Universität München, Boltzmannstraße 15, D-85748 Garching bei München, Germany

[2] Dipartimento di Scienze e Tecnologie Aerospaziali, Politecnico di Milano, Via La Masa 34, I-20156 Milano, Italy

E-mail: {johannes.schreiber, em.nanos, filippo.campagnolo, carlo.bottasso}@tum.de

Abstract. In this paper an adaptation of the FLORIS approach is considered that models the wind flow and power production within a wind farm. In preparation to the use of this model for wind farm control, this paper considers the problem of its calibration and validation with the use of experimental observations. The model parameters are first identified based on measurements performed on an isolated scaled wind turbine operated in a boundary layer wind tunnel in various wind-misalignment conditions. Next, the wind farm model is verified with results of experimental tests conducted on three interacting scaled wind turbines. Although some differences in the estimated absolute power are observed, the model appears to be capable of identifying with good accuracy the wind turbine misalignment angles that, by deflecting the wake, lead to maximum power for the investigated layouts.

1. Introduction

In a wind farm environment wind turbine wakes, which are characterized by a lower wind speed and higher turbulence intensity than the free steam, can adversely affect other turbines. This in turn may lead to higher fatigue loads and a significantly reduced power output on affected turbines.

To increase total wind farm power and/or reduce fatigue loads, several techniques have been proposed [1, 2]. At present, one of the most promising approaches seems to be a technique where the wake is deflected by operating the wind turbine in yaw-misalignment condition with respect to the incoming wind [3]. In fact, as the wind turbine is yawed out of the wind, its wake is laterally deflected, which may reduce its interaction with downstream machines. Wind farm control strategies based on wake deflection have been proposed to increase the total energy capture and/or decrease fatigue loading [3, 4]. In this context, reduced order wind farm models as the FLORIS (FLOw Redirection and Induction in Steady-state) approach [4] may be used to enable model-based wind farm control.

This paper describes first a FLORIS-like wind farm model. Next, its parameters are calibrated based on wake measurements of a scaled wind turbine in a wind tunnel environment. Finally, the tuned model is used to estimate the wind farm power output for several different wind farm layouts comprising three scaled interacting wind turbines. For each layout, a variety of different yaw-misalignment combinations are tested and the turbine power is compared to the model-predicted one. Results and the causes for the observed mismatches are discussed.

2. Wind farm model

In this section a reduced order wind farm model is presented, following the work of Gebraad et al. [4]. In the present study, the model has been re-implemented with some modifications. First, the model describing expansion, reduction and deflection of a single wind turbine wake is presented. Next, the models that describe wind turbine power extraction and multiple wake interactions are presented. Finally, the process of calculating wind farm flow and power is summarized.

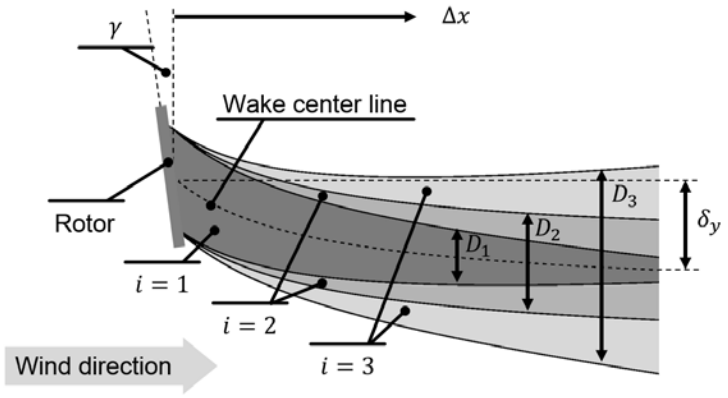

Figure 1. Wake model with three zones.

It is assumed that every wind turbine wake consists of three wake zones, as depicted in figure 1. In the generic wake zone i, the Jensen model [5] is used to describe wake expansion in terms of coefficient $k_{\mathrm{e},i}$. Experimental results suggest that the wake diameter of a turbine operated in a misaligned condition with respect to the wind direction is reduced (see the results section later on in this work). Taking this effect into account, the wake zone outer diameter is defined as

$$D_i(\Delta x, \gamma) = \max\left(0, (D + 2\Delta x k_{\mathrm{e},i})\cos(\gamma)^{k_{\mathrm{e},\gamma}}\right), \tag{1}$$

where Δx is the distance downstream of the wind turbine, D the rotor diameter, γ the wind turbine yaw-misalignment angle and $k_{\mathrm{e},\gamma}$ a parameter that describes the reduced wake expansion due to wind turbine yaw-misalignment. As the wake zones can have a negative expansion coefficient, the wake diameter has to be limited to positive values.

The wake velocity in each wake zone is described by the Jensen wake model as

$$U_i(\Delta x) = U_\infty\Big(1 - r_i(\Delta x)\Big), \tag{2}$$

where U_∞ is the ambient free stream velocity and r_i the reduction factor defined as

$$r_i(\Delta x) = 2a\left(\frac{D}{D + 2\Delta x k_{\mathrm{r},i}}\right)^2, \tag{3}$$

where a is the wind turbine induction and $k_{\mathrm{r},i}$ the wake reduction parameter of wake zone i.

The wake center line deflection due to yaw-misalignment is taken into account as described in [4], leading to

$$\delta_y(\Delta x, \gamma) = \frac{C_{\mathrm{T}}(\gamma)\left(15(2k_{\mathrm{d}}\frac{\Delta x}{D} + 1)^4 + C_{\mathrm{T}}(\gamma)^2\right)}{30\frac{k_{\mathrm{d}}}{D}(2k_{\mathrm{d}}\frac{\Delta x}{D} + 1)^5} - \frac{C_{\mathrm{T}}(\gamma)D\left(15 + C_T(\gamma)^2\right)}{30k_{\mathrm{d}}}, \tag{4}$$

where k_d is the single parameter describing the recovery of the wake flow direction and C_T the turbine thrust coefficient, which in turn is defined as a function of the rotor induction a and the yaw-misalignment as

$$C_T(\gamma) = \frac{1}{2}\cos(\gamma)^2 \sin(\gamma)\Big(4a(1-a)\Big). \tag{5}$$

For calculating the power extracted by a wind turbine, its rotor disk is split into m discrete elements e. The turbine power is obtained by summing up the power extracted in each element

$$P = \sum_{e=1}^{m} \frac{1}{2}\rho A_e C_\mathrm{P}(\gamma) V_e^3, \tag{6}$$

where ρ is the air density, A_e the element area, V_e the wind velocity at the discrete element and $C_\mathrm{P}(\gamma)$ the power coefficient expressed as a function of yaw-misalignment as

$$C_\mathrm{P}(\gamma) = C_{\mathrm{P},\gamma=0}\cos(\gamma)^{k_\mathrm{P}}. \tag{7}$$

Furthermore, $C_{\mathrm{P},\gamma=0}$ is the power coefficient of the turbine operating aligned with the wind, while k_p is the parameter taking into account power reduction due to yaw-misalignment. Speed V_e is calculated based on the wake deficits of all upstream turbines

$$V_e = U_\infty\left(1 - \left(\sum_{w=1}^{n} r_w^2\right)^{\frac{1}{2}}\right), \tag{8}$$

where n is the number of wake zones overlapping with the turbine rotor, while r_w the reduction factor of a wake zone impinging the element. In case $n = 0$, no wake is impinging on the element and therefore $V_e = V_\infty$.

The implemented algorithm is organized as follows. First, the power and wake characteristics of the first upwind turbine is calculated. In a second step, the next wind turbine is considered and the wake position, reduction, and expansion of all upwind turbines are interpolated at the given downwind position. Based on this, the turbine power can readily be computed by equation (6) and (8). Finally, the turbine wake is also computed, using equations (1,2) and (4), and the second step is repeated until the last turbine is reached.

3. Results

3.1. Experimental setup

The experiments described in this section were conducted with a scaled wind farm (see figure 2) composed of three identical scaled wind turbine models, longitudinally spaced 4 diameters (D) apart, whose rotor diameter is equal to 1.1 m (in the following named G1s for Generic 1 m diameter rotor), which were already used in other research projects [3, 6, 7]. The models were operated in the boundary-layer test section of the wind tunnel of the Politecnico di Milano, which has a cross-sectional area of 13.84 m by 3.84 m and a length of 36 m. Atmospheric boundary-layer conditions were simulated by the use of spires placed at the chamber inlet. The vertical profile of the longitudinal wind speed was measured prior to testing, resulting in the following best-fitted exponential law

$$U(z) = U_H\left(\frac{z}{z_H}\right)^{0.088}, \tag{9}$$

where $U_H \approx 5.7$ m/s and $z_H = 0.825$ m are the free-stream wind speed at hub height and the elevation of the rotor axis from the ground, respectively. The turbulence intensity (TI) at hub

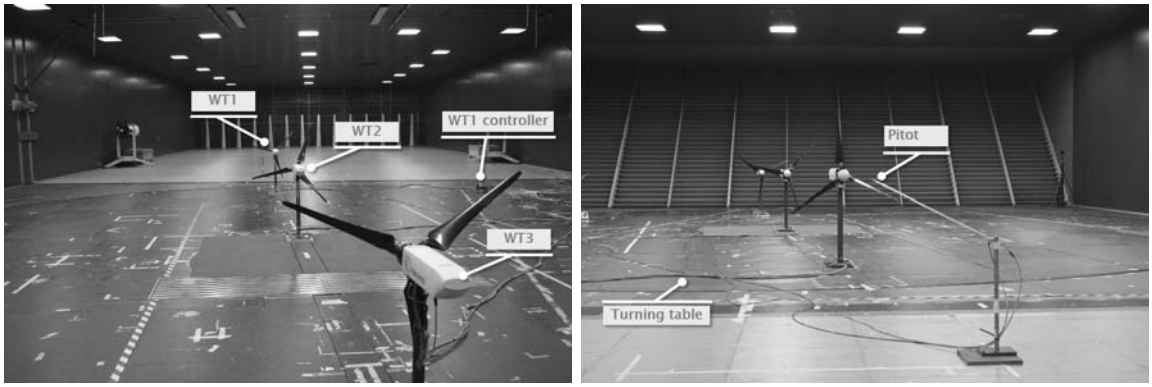

Figure 2. Wind farm layout in the wind tunnel.

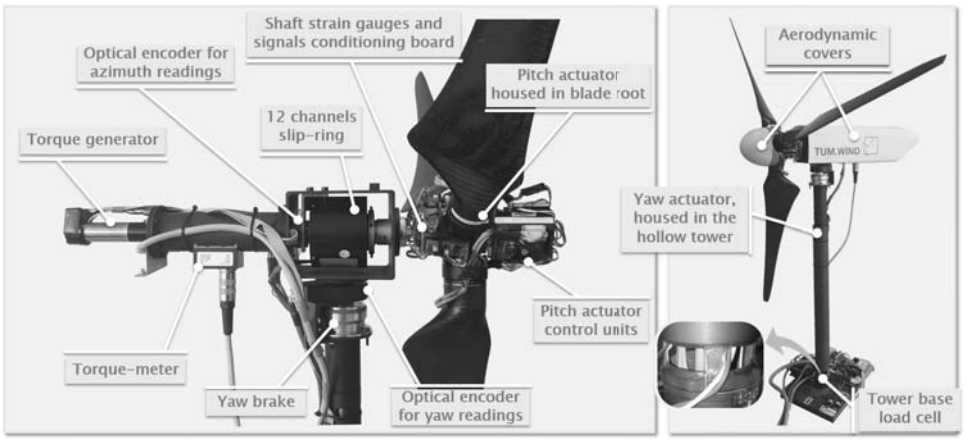

Figure 3. `G1` rotor-nacelle assembly (left) and overall model layout (right).

height was circa 5%. The undisturbed wind speed was measured by means of a pitot tube, also shown in figure 2, placed at hub height and 3D in front of the upstream model.

The dimensions of the model (see figure 3) are a compromise among the need for miniaturization, wind tunnel blockage, Reynolds effects and the need to realize multiple wind turbine interference conditions typical of wind farm operations. The scaled wind turbine is characterized by realistic aerodynamic performance, both at the airfoil and rotor levels, and generates a wake with shape, deficit and recovery that match closely the ones of a full scale machine. Moreover, the model features active individual pitch, torque and yaw control that, together with a comprehensive onboard sensorization of the machine (including measures of shaft and tower loads), enables the testing of modern control strategies.

Each model is controlled by a `M1 Bachmann` module that hard-real-time executes, similarly to what is done on real wind turbines, control laws similar to the ones described in [8] and references therein. In the present study, only operation below rated wind speed was considered. Therefore, the turbines were torque controlled according to a precomputed quadratic relation between rotor speed and torque.

3.2. Model parameter identification

For the identification of the model parameters, the wake velocity of an isolated G1 wind turbine was measured with hot wire probes and compared to model-predicted velocities. In the wind

conditions described above (TI of circa 5%), wake measurements were available at hub height at several downwind distances (3D, 4D, 6D, 9D). In this first set of experiments, no wake measurements in yawed condition had been conducted ($\gamma = 0$). Therefore, a second set of experiments had to be used for identifying the parameters that influence the wake in case of yaw-misalignment ($k_{\mathrm{e},\gamma}$ and k_{d}). In this second set of experiments, TI was much lower (TI of circa 1%), but the wind turbine was operated with yaw-misalignments between $-20° < \gamma < +20°$. The wake velocity was measured at a distance of 4D downwind of the wind turbine, again at hub height.

For the parameter identification, the hot wire velocity measurements V_{HW} were utilized to solve the minimization problem

$$\min_{p} \int \left(V_{\mathrm{HW}}(x) - V_{\mathrm{M}}(x,p)\right)^2 \,\mathrm{d}x, \tag{10}$$

where x is the lateral position of the measurement, V_{M} the model-predicted wake velocity for a set of model parameters p. The problem is solved by the Nelder-Mead simplex direct search algorithm implemented in the MATLAB function `fminsearch`. The wind turbine induction was obtained from a G1 blade element momentum simulation and set to $a = 0.35$ for operation below rated wind speed.

For the first set of experiments, the model parameters to be identified are defined as

$$p_1 = \{k_{\mathrm{e},1}, k_{\mathrm{e},2}, k_{\mathrm{e},3}, k_{\mathrm{r},1}, k_{\mathrm{r},2}, k_{\mathrm{r},3}\}. \tag{11}$$

Figure 4 shows the hot wire measurements $V_{\mathrm{HW}}(x)$ (red dashed line) and the model-predicted wake velocity $V_{\mathrm{M}}(x,p)$ (blue solid line) for the identified set of parameters. Only measurements at 4D were utilized for the identification (red solid line). The good quality matching of the profiles at 3D, 6D and 9D, since they were not used for calibrating the model, demonstrate its good generality.

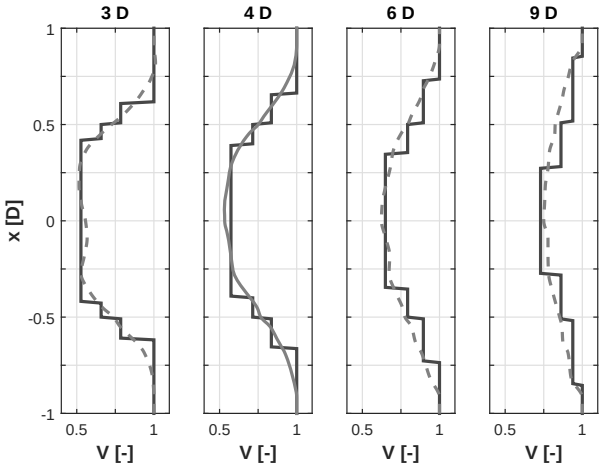

Figure 4. First measurement set (TI circa 5%), modeled (blue solid line) and measured (red solid and dashed lines) wake deficit for different distances behind the wind turbine.

To identify the wake parameters that play a role in turbine yaw-misalignment, the second set of experiments was used and the parameters to be identified by equation (10) were set to be

$$p_2 = \{k_{\mathrm{e},\gamma}, k_{\mathrm{d}}\}. \tag{12}$$

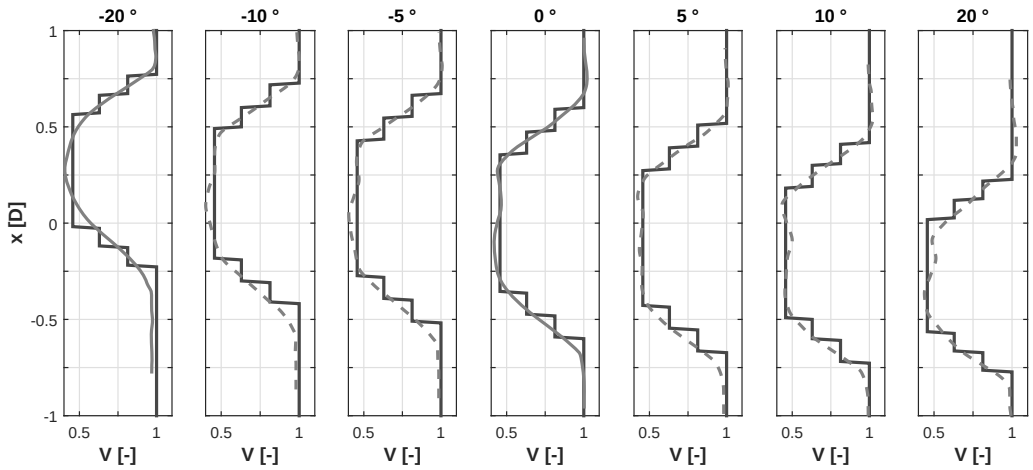

Figure 5. Second measurement set (TI circa 1%), modeled (blue solid line) and measured (red solid and dashed lines) wake deficit for different yaw-misalignments.

The parameters p_1 were re-identified for the low TI case to take the slower wake recovery of this different flow condition into account. Figure 5 shows the hot wire measurements $V_{\mathrm{HW}}(x)$ and the model-predicted wake velocity $V_{\mathrm{M}}(x, p)$ for the identified set of parameters. Again, the generality of the wake model is demonstrated by only taking the measurements of $\gamma = -20°$ and $\gamma = 0°$ into account during the identification. Note the wake diameter reduction in the cases characterized by larger yaw-misalignment. The modeled maximum wake diameter for $\gamma = 0°$ is 1.2D, whereas for $\gamma = \pm 20°$ the wake diameter is only 1D, giving a good fit with the wake measurements.

It is assumed that the parameters $k_{\mathrm{e},\gamma}$ and k_{d} are independent of TI. Therefore, they can be used to describe the wake also for the higher TI cases used in the wind farm experiments.

Parameter k_{p} was identified based on a subset of the wind farm experiments in which the first turbine yaw-misalignment was $-36° < \gamma < 0°$. In this subset, the first wind turbine experimental power coefficient $C_{\mathrm{P,Exp}}(\gamma)$ was calculated based on turbine power measurements and pitot tube measurements 3D in front of the hub, as shown in figure 6 (red circles). The squared error between the measured and modeled power coefficients, given by equation (7), was minimized with respect to the free parameters k_{p} and $C_{\mathrm{P},\gamma=0}$, yielding the modeled power coefficient shown in figure 6 (blue solid line). Coefficient $C_{\mathrm{P},\gamma=0}$ was included in the free parameters to account for a low precision in the pitot tube measurements.

The full set of identified model parameters is reported in Table 1. For the sake of completeness, Table 1 also reports the identified parameters for low TI, which correspond to Figure 5.

Table 1. Identified model parameters.

	$k_{\mathrm{e},1}$	$k_{\mathrm{e},2}$	$k_{\mathrm{e},3}$	$k_{\mathrm{r},1}$	$k_{\mathrm{r},2}$	$k_{\mathrm{r},3}$	$k_{\mathrm{e},\gamma}$	k_{d}	k_{p}
high TI	-0.0251	0.0011	0.0386	0.0320	0.0669	0.2130	2.8808	0.1219	1.7870
low TI	-0.0363	-0.0062	0.0236	0.0140	0.0433	0.1864	2.8808	0.1219	1.7870

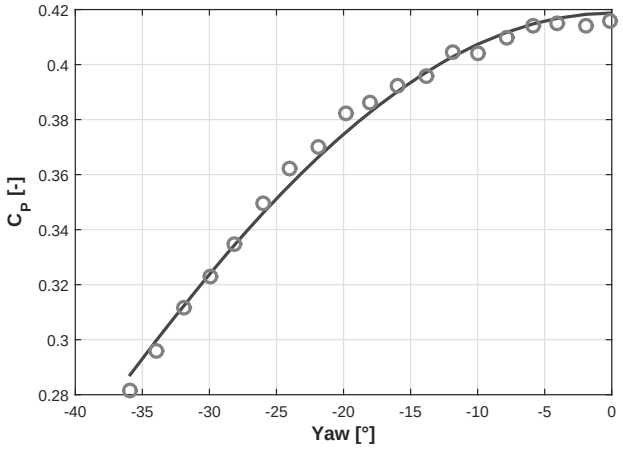

Figure 6. Measured (red circles) and modeled (blue solid line) power coefficients plotted as functions of wind turbine yaw-misalignment.

3.3. Wind farm experiments

In the wind farm experiments, three G1s were operated in the wind tunnel in three different layouts (noted A, B and C) as shown in figure 7. In each layout, the most upwind wind turbine is labeled WT1, the middle turbine is noted WT2, while the most downwind wind turbine is termed WT3. The turbines were torque controlled below rated wind speed, and the reduced order model assumed a constant operation of all turbines with $C_{\mathrm{P},\gamma=0} = 0.419$ and $a = 0.35$.

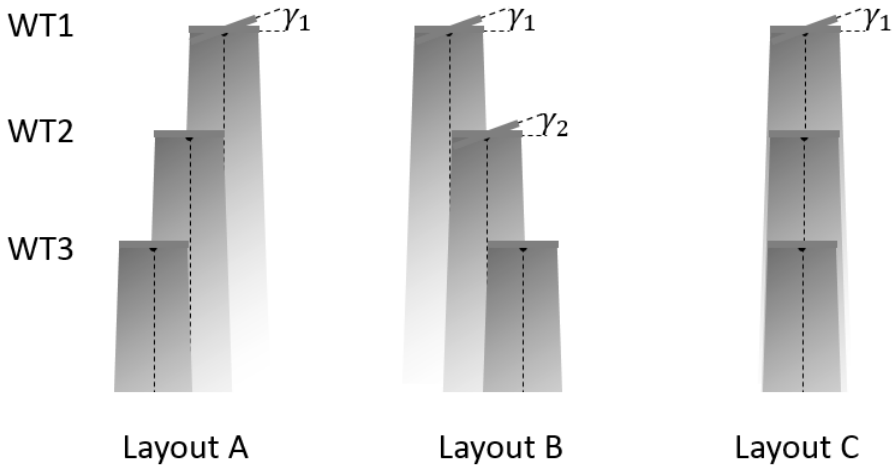

Figure 7. Wind farm layouts A, B, C with lateral displacements of ±0.5D and 0D. The longitudinal displacement is approximately 4D. Note that the sketch is not to scale.

First, for every layout several experiments were conducted with different yaw-misalignments of WT1 (γ_1), in order to deflect the wake away from the downstream turbines. For these experiments, figure 8 shows the power coefficient of all three wind turbines and the total wind farm in layouts A, B and C, as indicated by the column title. The red circles indicate the measured and the blue solid line the modeled power coefficient, respectively.

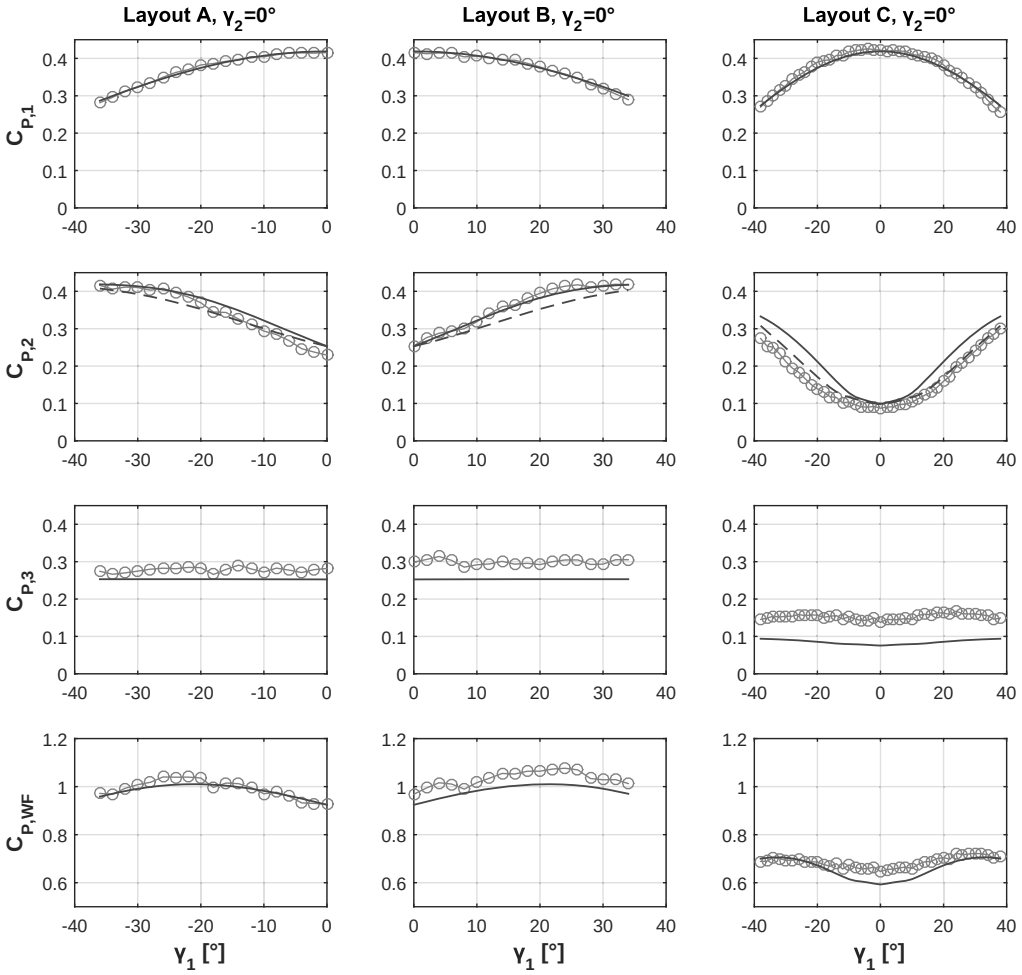

Figure 8. Measured (red circles) and modeled (blue solid line) power coefficient for WT1, WT2, WT3 and the total wind farm, for layouts A, B and C.

The first row of subplots shows the power coefficient of WT1 ($C_{\mathrm{P},1}$) in each layout. As expected from the identification of parameter k_{p}, the model-predicted and measured results correlate very well.

The second row of subplots shows the power coefficient of WT2 ($C_{\mathrm{P},2}$). For $\gamma_1 = 0°$, the model predicts well the downwind turbine power for all layouts. However, a small asymmetric behavior in the measurements can be observed between the symmetric layouts A and B — perhaps due to asymmetric wake behavior or due to a small horizontal variation in the wind tunnel inflow speed. In the experiments of layout B, maximum power is reached already at $\gamma_1 \approx 25°$ and further upwind turbine yawing does not influence the second wind turbine power anymore. In the full wake case of layout C, the model significantly over-predicts power for $|\gamma_1| > 10°$. A first hypothesis that could explain this behavior is that the model predicts a slightly inaccurate wake location in the yawed cases (which is possible, given that the corresponding parameter was identified at a much lower TI). Indeed, simulations with a larger wake deflection parameter ($k_{\mathrm{d}} = 0.28$, see blue dashed line) show improved results for layout C, but the new parameter

affects also the results in layouts A and B, where now the modeled power coefficient exhibits an increased error. Results in layout C might improve by adjusting the model in such a way that in yaw-misalignment conditions the wake speed decreases or the wake diameter reduces further than currently predicted, but this would worsen the results in layouts A and B. The previously mentioned slight lateral variation in the inflow speed, which cannot be captured by the use of a single pitot tube, could also be a partial cause of the mismatch seen here. It is also possible that the wake deflection position is affected by the downwind turbine position. Understanding the reasons causing these discrepancies will be part of further studies, involving additional wind farm flow measurements.

The third row of subplots shows the power coefficient of WT3 ($C_{\mathrm{P},3}$). In layout A and B, no significant γ_1-dependency can be observed in the experiments as well as in the model. Nevertheless, the power is constantly under-predicted. The cause might be a faster wake recovery of the wake of WT2 that, operating within the wake of WT1, experiences a higher turbulence intensity, leading to a faster wake mixing. Conversely, a strongly deflected wake (i.e. $|\gamma_1| > 25°$) should in that case also lead to lower power at WT3 — an effect that however is not observed in the experiments. Again, further studies and measurements are necessary to better explain this contradiction. For layout C, the power of WT3 is clearly affected by γ_1. The model correctly predicts an increase of power for increased γ_1. However, above $|\gamma_1| > 20°$ the experimental results show a decrease of power, which might be caused by a slower wake recovery of the WT2 wake compared to the full wake case ($\gamma_1 = 0$).

The total power coefficient of all three wind turbines ($C_{\mathrm{P,WF}} = C_{\mathrm{P},1} + C_{\mathrm{P},2} + C_{\mathrm{P},3}$) is shown in the last row of figure 8. Taking into account the discrepancies noted above, the overall correlation is rather good. In layouts A and B the predicted power achieves a maximum for $|\gamma_1| = 20°$, which correlates well with the experimental data. In the full wake case, the predicted power is maximum at $|\gamma_1| = 34°$, which again correlates well with the experimental data.

For layout B, experiments were also conducted in which WT2 is operating in yaw-misalignment (γ_2). Figure 9 shows experiments in which WT2 is yawed by $\gamma_2 = 8°$ (first column), $\gamma_2 = 18°$ (second column) and $\gamma_2 = 28°$ (third column). The power of WT1 is again well predicted. For WT2 the modeled and measured power decreases for increased γ_2, even though the model under-predicts this effect slightly at higher γ_2. The power of WT3 increases as expected with increased γ_2. Surprisingly, for $\gamma_2 = 28°$ the WT3 power exceeds the maximum power coefficient in four experiments — possibly due to a flow acceleration just outside of the wakes of WT1 and WT2. The total power of all three turbines follows the trend of the experiments, but the previously observed power over-prediction becomes smaller for increased γ_2, mainly due to the under estimation at WT2 and the smaller error at WT3.

The full set of experiments, not shown here for brevity, includes all combinations of γ_1 and γ_2 in steps of 2° around the point of maximum power. By using this data, the experimental optimum yaw configuration could be readily identified and was found to be at $\gamma_1 = 20°$ and $\gamma_2 = 16°$. The model-predicted point of maximum wind farm power was on the other hand found to be located at $\gamma_1 = 20°$ and $\gamma_2 = 22°$.

4. Conclusions and outlook

In this paper, the parameters of a reduced order wind farm model were identified with the help of wake measurements along a hub-height horizontal line for an isolated wind turbine. The modeled wakes are in good agreement with the measurements, even though only a small subset of the measurements were taken into account for the model identification procedure.

For three different wind farm layouts, including a variety of yaw angles of the two upstream wind turbines, the model-predicted wind turbine power coefficient was compared with experimental measurements. The comparison shows a good correlation in the overall trends, but the absolute values are not always well predicted especially for the last downstream wind turbine.

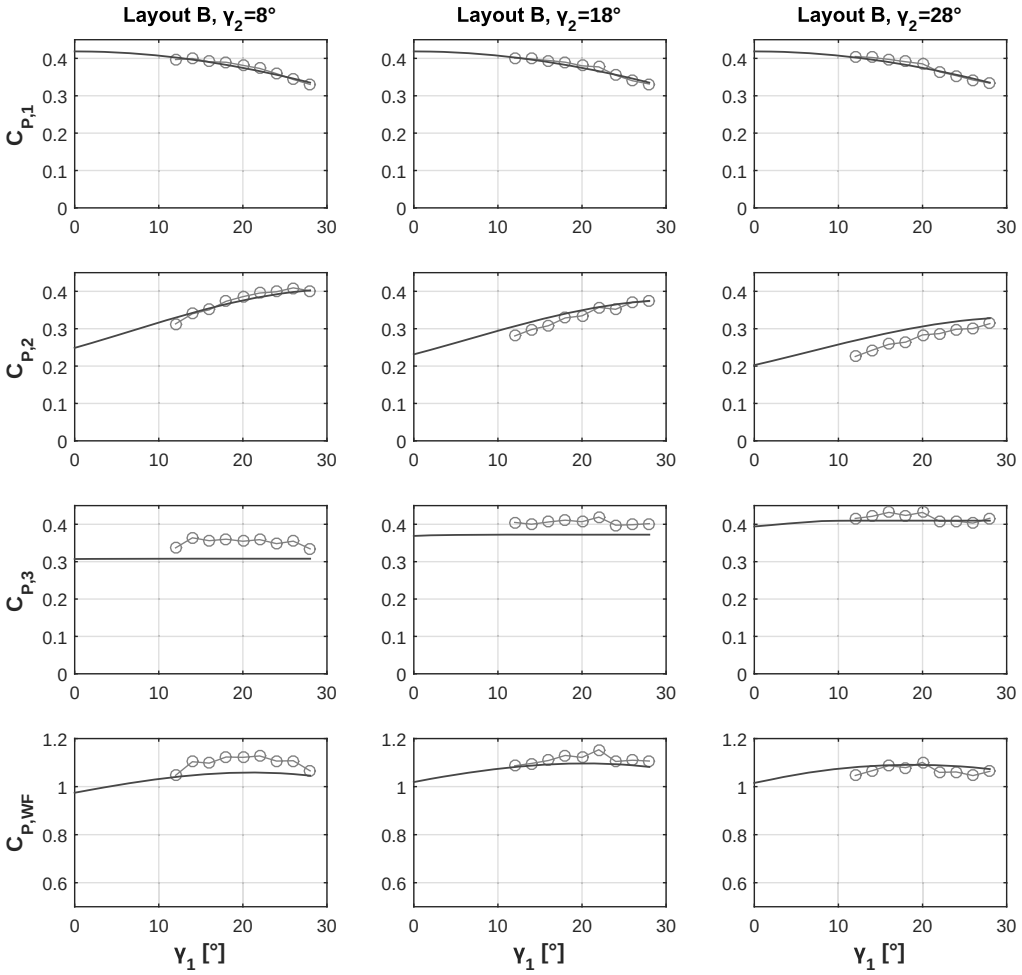

Figure 9. Measured (red circles) and modeled (blue solid line) power coefficient for WT1, WT2, WT3 and the total wind farm, for layout B for different γ_2 values.

The causes are believed to be a combination of various effects, including a faster recovery of wakes shed by waked turbines, flow acceleration outside the wakes, lateral flow speed variations in the wind tunnel, Reynolds number effects in the experiments, the assumption of a uniform power coefficient on each rotor, the assumption of axisymmetric wakes and certainly additional not modeled and fully understood effects like the influence of the downwind turbines on the upstream wake development.

Regardless of these open questions, it is important to note that the employed rather simplistic wind farm model, after a tuning by wake measurements, predicts well the operating point of maximum wind farm power. This is a promising result in view of the use of the model for wind farm control. It is also worth noting that the power gradient is very small around the optimum yaw angles for all studied layouts, implying that for wind farm control purposes a rough estimation of the optimum yaw configuration should be enough to harvest most of its potential.

Future work will try to clarify the open points and improve the model, taking into account

the various deficiencies stated above. In addition, rotor load-based wind estimation and wake detection techniques [9] will be coupled with the model for the development of robust model-based closed-loop wind farm control.

Acknowledgments

The authors wish to thank Dr. Vlaho Petrović for his help in the preparation and realization of the experiments, and Mr. Amr Balbaa for the assistance with the parameter identification.

This research was partially supported by the European Union Horizon 2020 research and innovation program under the Marie Skłodowska-Curie grant agreement No. 642108, and it was also partially supported by the German Federal Ministry for Economic Affairs and Energy (BMWi) within the CompactWind project (FKZ: 0325492D).

References

[1] Wang J, Bottasso C L and Campagnolo F 2016 Wake redirection: comparison of analytical, numerical and experimental models *Journal of Physics: Conference Series* **753** 32064

[2] Fleming P A, Gebraad P M O, Lee S, van Wingerden J-W, Johnson K, Churchfield M, Michalakes J, Spalart P and Moriarty P 2014 Evaluating techniques for redirecting turbine wakes using SOWFA *Renewable Energy* **70** 211-8

[3] Campagnolo F, Petrović V, Schreiber J, Nanos E M, Croce A and Bottasso C L 2016 Wind tunnel testing of a closed-loop wake deflection controller for wind farm power maximization *Journal of Physics: Conference Series* **753** 32006

[4] Gebraad P M, Teeuwisse F W, Van Wingerden J W, Fleming P A, Ruben S D, Marden J R and Pao L Y 2016 *Wind Energy* **19** 95–114 ISSN 10954244

[5] Jensen N O 1983 A note on wind generator interaction (Roskilde, Denmark: Risø National Laboratory)

[6] Campagnolo F, Petrović V, Bottasso, C L and Croce A 2016 Wind tunnel testing of wake control strategies *Proceedings of the American Control Conference* 513–518

[7] Campagnolo F, Petrović V, Nanos E M, Tan C W, Bottasso C L, Paek I, Kim H and Kim K 2016 Wind tunnel testing of power maximization control strategies applied to a multi-turbine floating wind power platform *Proceedings of the International Offshore and Polar Engineering Conference* 309–316

[8] Bossanyi, E 2000 The design of closed loop controllers for wind turbines *Wind Energy*, **3** 149–163.

[9] Schreiber J, Cacciola S, Campagnolo F, Petrović V, Mourembles D and Bottasso C L 2016 Wind shear estimation and wake detection by rotor loads - First wind tunnel verification *Journal of Physics: Conference Series* **753** 32027